Journal of Applied Electrochemistry **33**: 733–739, 2003.

The effect of current density on properties of electrodeposited nanocrystalline nickel

F. EBRAHIMI* and Z. AHMED
*Materials Science and Engineering Department, University of Florida, PO Box 116400, Gainesville, FL 32611, USA (*author for correspondence, fax: +352 846 3355, e-mail: febra@mse.ufl.edu)*

Received 30 September 2002; accepted in revised form 26 March 2003

Key words: electrodeposition, fracture, nanocrystalline nickel, tensile properties

Abstract

Nanocrystalline nickel electrodeposits were fabricated at 18, 25 and 50 mA cm^{-2} using a sulfamate-based electrolyte. The crystallite size of the deposits was evaluated by XRD technique and their mechanical properties were characterized by tensile testing. The results of this study confirmed that increasing the current density results in an increase in the grain size of nickel deposits. The strength of the deposits decreased consistently with increasing the crystallite size. However, the deposit fabricated at 50 mA cm^{-2}, in comparison to nickel with conventional grain size (>1 μm), showed a relatively low strength and a surprisingly low tensile elongation. It is suggested that the enhanced evolution of hydrogen at high current densities is responsible for the formation of larger crystals and the unusual low tensile elongation.

1. Introduction

Electrodeposition is a feasible and inexpensive method to fabricate strong and relatively ductile metallic nanostructures [1]. Many parameters are involved in the electrodeposition process, including type of electrolyte, concentration of ions, pH, bath temperature, degree of agitation, substrate and counter electrode geometry and material, overpotential and/or current density, mode of deposition (d.c. *versus* pulse plating or galvanostatic *versus* potentiostatic), and presence of additives in the electrolyte. Conventionally, the electrodeposits have columnar grains, whose diameters increase with the deposit thickness [2]. In order to obtain equiaxed nanocrystals, continuous nucleation of new grains should occur during the deposition. In general, factors that promote the formation of defects (e.g., dislocations and twins) tend to reduce the crystallite size of metallic deposits [2,3]. The addition of foreign molecules is the most widely used method for controlling the quality of coatings [4]. For example, the grain size of nickel can easily be reduced into nanorange (<100 nm) by using additives such as coumarin and saccharin [5]. However, these additives result in a high concentration of surface-active elements such as sulfur and carbon, which can easily segregate to grain boundaries and weaken them.

We have been successful in fabricating nanocrystalline nickel using a sulfamate-based solution without grain-refining additives [6]. The pH of the solution was found to play an important role on the crystallite size. A pH in the range of 4.6 to 4.8 has been established to result in the finest crystallite size at a current density of 18 mA cm^{-2} for our cell set-up. At this current density, the average crystallite size varied from 38 nm at pH of 4.7 to 342 nm at the pH of 2.4. Therefore, the control of pH is essential for obtaining nanosize grains in nickel deposits.

A high current density is also anticipated to promote grain refinement. An increase in the current density is expected to result in a higher overpotential, which should increase the nucleation rate [7]. However, surprisingly, Cziraki et al. [8] have reported that increasing the current density from 100 to 500 mA cm^{-2} using a sulfate-based solution results in an increase in the grain size of d.c.-electroplated nickel. The objective of this study was to investigate the effect of current density on the crystallite size, texture and tensile properties of electrodeposited nanocrystalline nickel using a sulfamate-based solution.

2. Experimental procedures

A conventional rotating disc set-up was employed for the deposition of nickel specimens [9]. The electrolyte was a sulfamate solution consisting of 90 g l^{-1} Ni, 30 g l^{-1} boric acid and 0.075 g l^{-1} SNAP (sulfamate-nickel-anti-pit). SNAP facilitates the removal of hydrogen bubbles form the deposit front and does not get incorporated into the deposit [10]. The pH of the as-made solution was raised to within the optimum range of 4.6 to 4.9 by adding about 1.5 g l^{-1} nickel carbonate. The solution was heated to approximately 50 °C in order to expedite the dissolution. After cooling to room

temperature, the solution was filtered in order to remove the un-dissolved particles. The pH was measured at room temperature.

The substrate was an annealed 100 μm thick copper disc with a 35 mm diameter. The copper substrate had a strong $\{100\}\langle 001\rangle$ texture. The counter electrode was a 10 cm $\times$ 10 cm^2 platinum foil. Nickel was deposited galvanostatically at 18, 25 and 50 mA cm^{-2} current densities at 30 °C. A PAR 273 potentiostat/galvanostat, which was interfaced with a computer, was used for controlling and recording current or potential. The potential was measured against a saturated calomel electrode (SCE). The tip of the reference electrode was located at the level of the substrate and very close to the surface of the rotating cathode. Prior to deposition, the substrate was electropolished potentiostatically at an anodic voltage of 1.1 volts for about 17 min using a solution consisting of 82.4% phosphoric acid and 17.5% deionized water at room temperature and then activated in a 10% sulfuric acid solution. The deposition time was adjusted such that based on 100% efficiency and using Faraday's law, 50 μm deposits would be obtained. Cyclic voltammetry between 0 and −2 V at a rate of 11 mV s^{-1} was performed to evaluate the current–potential relationship and the limit current density. The voltammetry was conducted after depositing a layer of nickel.

After deposition, the electrodeposited discs were cut into four strips and then the copper substrate was chemically dissolved. The strips were always cut along the rolling direction of the copper substrate in order to assure that in the presence of in-plane texture of the deposits, the tensile samples were loaded along a similar orientation. Dog-bone shaped tensile specimens with 10 mm gauge lengths were prepared by careful grinding and tested at a nominal strain rate of 2×10^{-4} s^{-1} using pneumatic grips. At least two tensile samples per deposit were tested. X-ray diffraction (XRD) technique was employed for characterizing the texture and evaluating the crystallite size of deposits. The Warren–Averbach method using (200) and (400) reflections was employed for estimating the crystallite size of deposits. The Line Profile software that accompanies the Philips APS 3720 system was used for analysis. Since the texture and crystallite size vary through the thickness of deposits, they were measured on both the substrate and the solution side of the deposits. The surfaces of deposits as well as the fracture surfaces of tensile specimens were characterized in the JEOL 6400 SEM (scanning electron microscope).

3. Results and discussion

3.1. *Cyclic voltammetry and transient curves*

Cyclic voltammetry was conducted to measure the limit current under the deposition conditions used in this study in order to avoid diffusion controlled deposition.

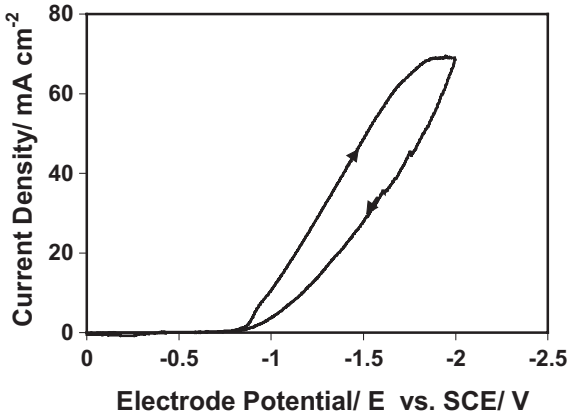

Fig. 1. Voltammogram for deposition of nickel on nickel in the sulfamate solution with pH of 4.7 at the scan rate of 11 mV s^{-1}.

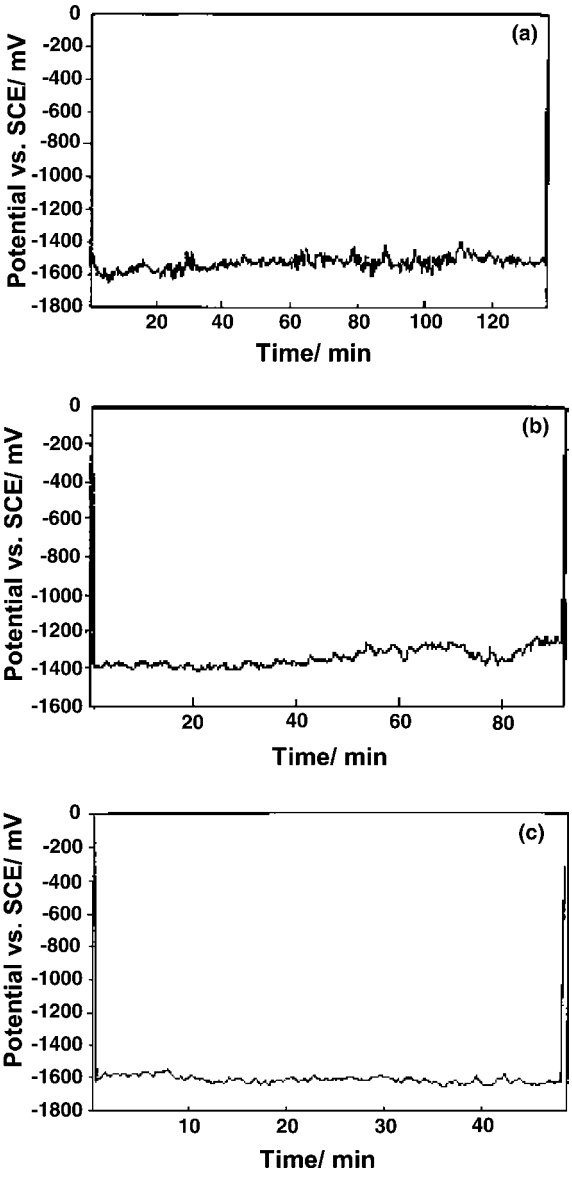

Fig. 2. Transient curves for samples deposited at different current densities: (a) 18, (b) 25 and (c) 50 mA cm^{-2}.

Table 1. Summary of the results of microstructural analysis of the nickel deposits ($I_{(200)}/I_{(111)}$ for a completely random orientation of grains for nickel is 0.46)

Current density /mA cm^{-2}	pH	Potential vs SCE /V	Thickness /μm	Efficiency /%	$I_{(200)}/I_{(111)}$		Crystallite size /nm	
					sub	*sol*	*sub*	*sol*
18	4.66	−1.6 to −1.4	37.5	75	42	3	111	11
25	4.71	−1.4 to −1.25	30	60	54	5	35	17
A-50	4.91	−1.7	26	52	8	6	103	66
B-50	4.76	−1.6	24	48	81	76	*NA*	55

NA – Not analysed because the grains on the substrate side of sample B were too large for accurate measurement by XRD.

The limit current at 400 rpm cathode rotation, which was used during the deposition of nanocrystalline nickel samples, was outside the capacity of our system (>100 mA cm^{-2}). Figure 1 presents the current density–potential curve for a stationary electrode at 30 °C in the nickel sulfamate solution used in this study with a nickel deposit as substrate. The limit current under this condition was 72 mA cm^{-2} and nickel deposition started at about −0.8 V against the SCE ($V_{SCE} = 0.2415$ V vs SHE, standard hydrogen electrode). These observations confirm that the current densities used in this study were much less than the diffusion-limited current density.

Figure 2 presents the transient curves during the d.c. deposition of the nickel samples. Note that the deposition time was adjusted to achieve equal deposit thickness values based on the Faraday's law. The potentials obtained at 25 and 50 mA cm^{-2} are consistent with the voltammetry results (see also Table 1). However, an unexpectedly higher electrode potential was measured at 18 mA cm^{-2} current density. The efficiency, as defined by the ratio of the deposit thickness to the calculated thickness (using Faraday's law), decreased with increasing the current density, independent of the average deposition potential. Also, as the current density was decreased the variations in the potential became larger as indicated by the waviness of the potential – time curves. These potential spikes are associated with the cathode rotation and reflect the transport of the metal ions to the cathode surface. The fact that they are more pronounced at lower current densities indicate that under these conditions the ion transport is more controlled by the convection than by the diffusion processes. As the current density was increased to 50 mA cm^{-2}, the reaction rates at the cathode surface were forced to increase, and hence, the transport of the ions through the diffusion layer became more important. Consequently, the potential was less sensitive to the transport of the ions by the convection mechanism.

3.2. *Microstructural characterization*

Table 1 presents the results of microstructural analysis. Two deposits were made at 50 mA cm^{-2}. The main difference between the two deposits is a slight variation in the pH of the solutions, and as can be seen in Table 1 the results for them are similar. These findings show that increasing the current density from 18 to 50 mA cm^{-2} resulted in coarsening of the crystallite size. This observation is consistent with the results reported by Cziraki et al. [8], who used a sulfate-based electrolyte and current densities in the range 100 to 500 mA cm^{-2}.

All deposits showed a tendency toward (100) texture as indicated by the $I_{(200)}/I_{(111)}$ X-ray peak ratios. The X-ray analysis was conducted on both the solution and substrate sides of the freestanding deposits. The crystallite size was larger on the substrate side of all deposits. Except for one of the deposits made at 50 mA cm^{-2} (sample A), the deposits showed a strong (100) crystallographic texture on the substrate side. This phenomenon can be partially attributed to the mimicking of the surface structure of the copper substrate, which had a very strong (100) texture [12]. To evaluate the variations of texture and crystallite size through the thickness of deposits, a sample of the deposit made at 25 mA cm^{-2} was carefully ground from the solution side and the X-ray analysis was conducted after the removal of every few micrometres. Figure 3 presents the change in the crystallite size and the $I_{(200)}/I_{(111)}$ ratio as a function of distance from the substrate side. There is an excellent correlation between the variations of texture and crystallite size. Both showed a change when the distance from the substrate was approximately 10 μm.

Nickel deposits made from sulfamate solutions grow preferentially along the ⟨100⟩ directions [6]. The decrease in the crystallite size and the associated loss of texture with the growth of the deposits is unique to the nanocrystalline deposits [6] and is contrary to the behaviour of deposits with large grain sizes [2]. If the grains grow in a columnar manner both the average grain diameter and the degree of texture increase as the deposit thickens. However, in the case of nanostructures, where the continuous nucleation of new grains occurs, the grain size as well as the severity of texture decreases through the thickness of the deposit. Our recent results [12] indicate that the use of cold-rolled copper substrate with a {110}⟨112⟩ texture may suppress the ⟨100⟩ texture on the substrate side but will not eliminate it.

The increase in the crystallite size associated with increasing the current density caused rougher surfaces as viewed on the solution side. Figure 4 presents the SEM

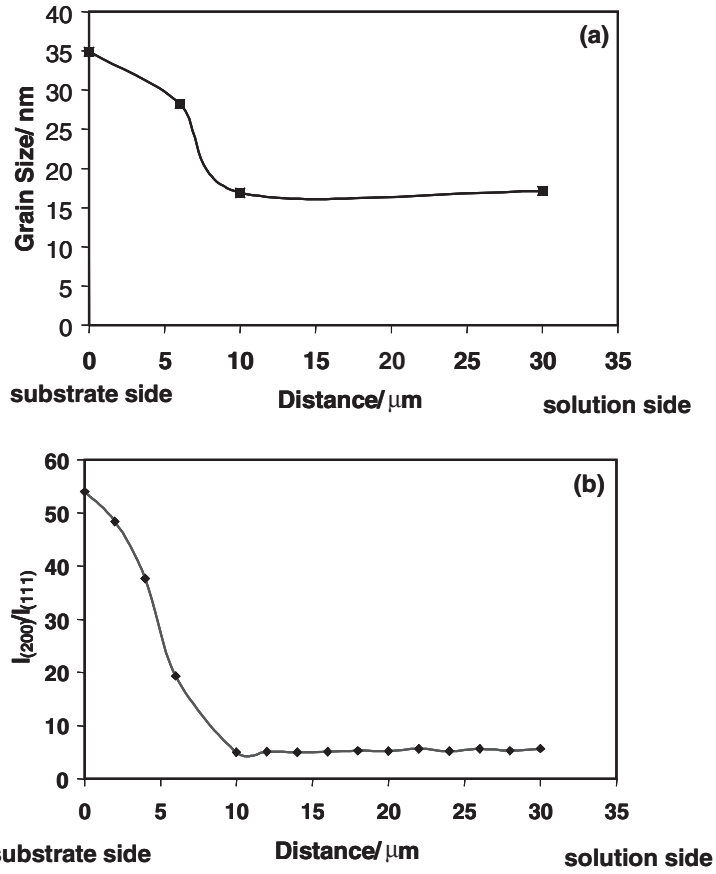

Fig. 3. Variations of (a) grain size and (b) $I_{(200)}/I_{(111)}$ ratio through the thickness of the nickel deposit made at 25 mA cm^{-2}.

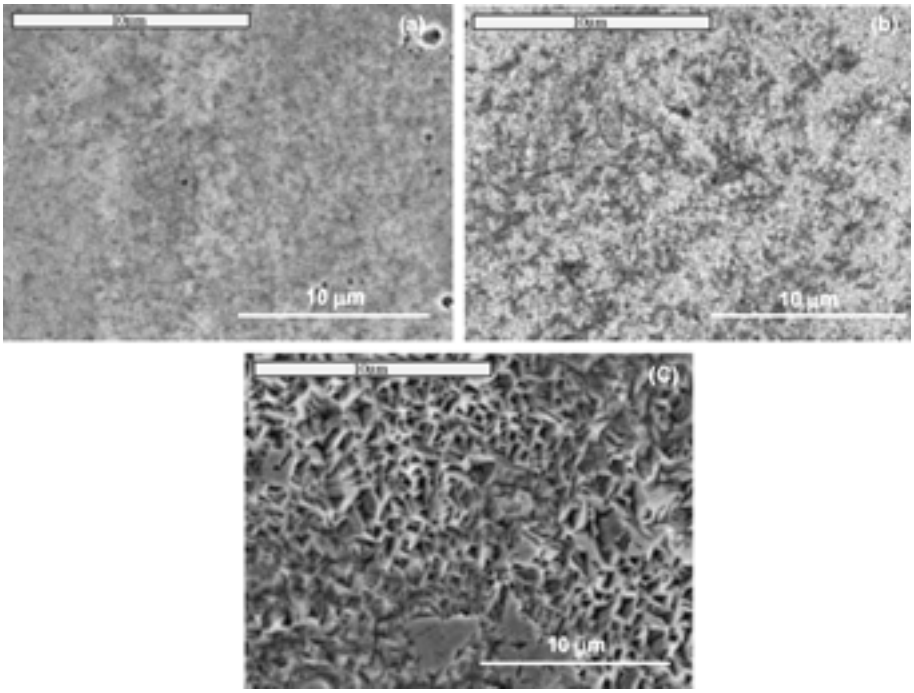

Fig. 4. SEM micrographs from the surfaces of samples deposited at different current densities: (a) 18, (b) 25 and (c) 50 mA cm^{-2}.

pictures from the surface of the deposits. It should be noted that the apparent roughness observed on the surface is related to the crystallite size but is usually much larger than the actual crystallite size. For example

Table 2. Summary of the tensile properties of the d.c. electrodeposited nickel (where e_f^p is the plastic component of the total tensile elongation)

Current density /mA cm^{-2}	Specimen	$\sigma_{0.2\%}$ /MPa	$\sigma_{1\%}$ /MPa	σ_{UTS} /MPa	e_f^p /%	e_f /%
18	1	561	–	977	0.9	2.4
	2	630	982	1102	1.2	2.9
25	1	593	1018	1285	4.6	6.2
	2	667	1062	1300	2.4	4.8
50	1	259	339	386	1.8	2.4
	2	203	–	247	0.35	0.9
50	1	271	305	305	1	1.9
	2	243	297	299	1.3	2.5

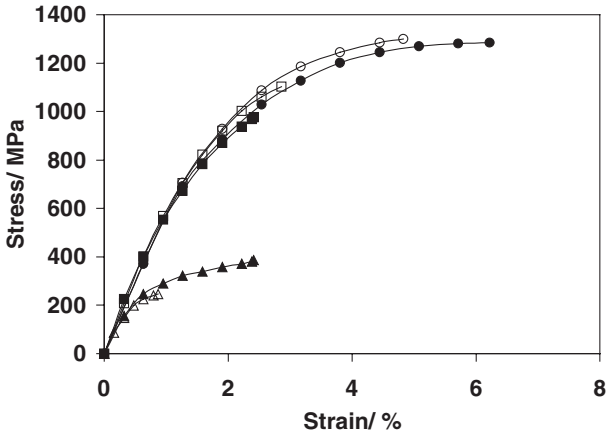

Fig. 5. Tensile stress–strain curves. Current densities for specimens (1, 2), respectively: (▲, △) 50, (■, □) 18 and (●, ○) 25 mA cm^{-2}.

the apparent roughness on the surface of the deposit made at 50 mA cm^{-2} is about micrometer size but the crystallite size is an order of magnitude smaller.

3.3. *Tensile properties*

The results of the tensile testing are summarized in Table 2 and the stress–strain curves are given in Figure 5. The $\sigma_{0.2\%}$ is the stress at 0.2% plastic strain and represents the yield strength of the material. The $\sigma_{1\%}$ is the value of stress at 1% plastic strain and the ultimate tensile strength σ_{UTS} is the stress at the point of fracture. Consistent with the change in the crystallite size the strength of the deposits decreased with increasing the current density.

The relationship between the strength and grain size is conventionally expressed as the Hall–Petch equation:

$$\sigma = \sigma_i + Kd^{-1/2}$$

where d is the grain size, σ_i is the friction stress representing the stress required to move dislocation within the crystal and k is a material constant, which represents the effectiveness of the grain boundaries in strengthening. Figure 6 shows the strength as a function of $d^{-1/2}$ for the results obtained in this study. In comparison to the yield strength values, the slope of the curve is higher for the flow stress at 0.1% strain,

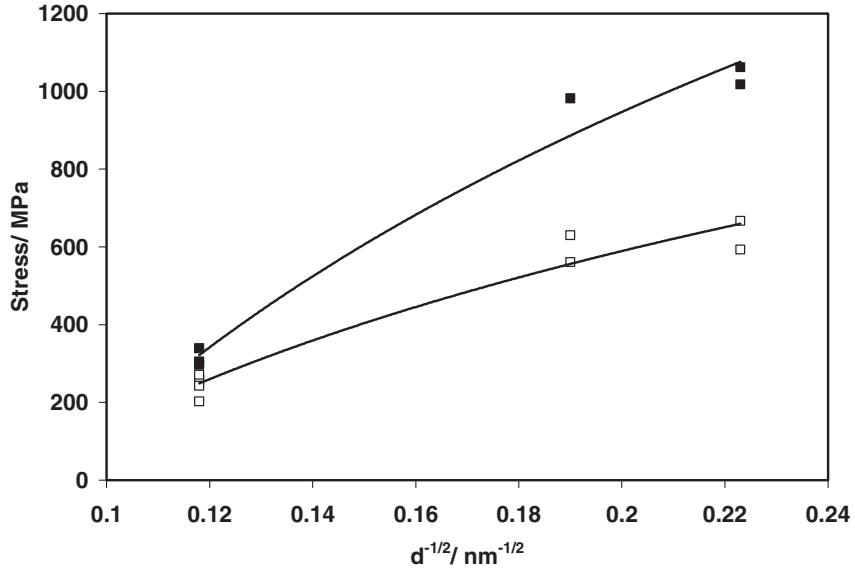

Fig. 6. $\sigma_{0.2\%}$ (open symbol) and $\sigma_{1\%}$ (filled symbol) as a function of $d^{-1/2}$.

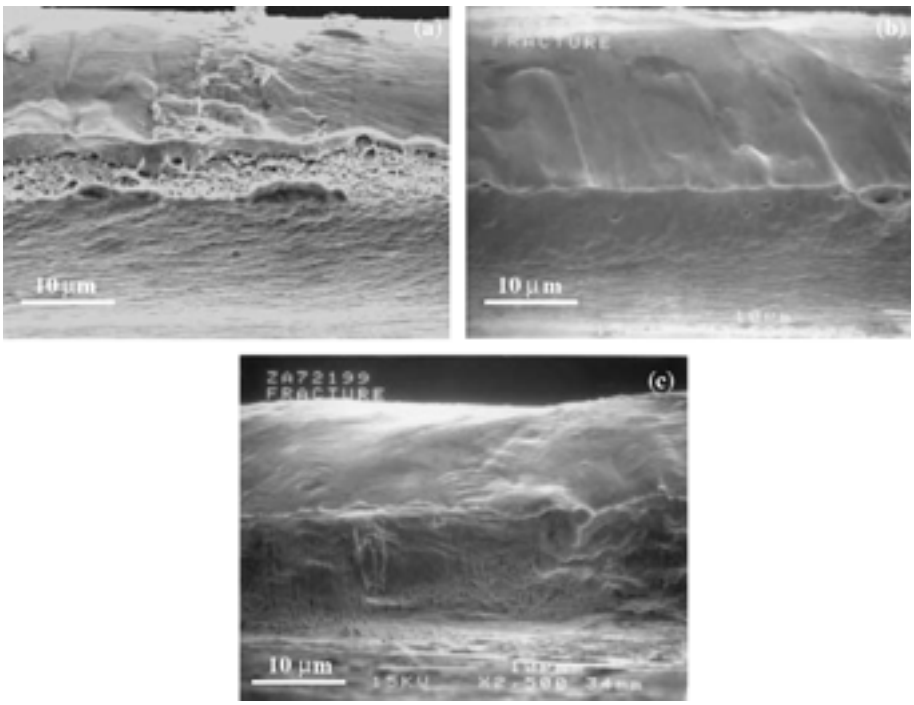

Fig. 7. SEM pictures from the fracture surface of samples deposited at different current densities: (a) 18, (b) 25 and (c) 50 mA cm^{-2}.

indicating that the strain-hardening rate increases with decreasing the grain size. The slope becomes less steep at smaller grain sizes, a phenomenon often reported in metallic nanocrystals [13]. Besides the deformation mechanism, several parameters may contribute to this change in slope, including an increase in the width of the grain size distribution and changes in the grain boundary structure as the grains become smaller.

The fracture surfaces are shown in Figure 7. All samples fractured in a ductile manner as evidenced by the knife-edge fracture behaviour in samples deposited at 25 mA cm^{-2} and 50 mA cm^{-2} and the microvoid coalescence mechanism in samples deposited at 18 mA cm^{-2}. The initiation of microvoids that lead to the fracture of electrodeposits is attributed to the entrapment of hydrogen bubbles at the deposition front [14]. Factors such as local pH, surface tension of the cathode and the electrolyte flow near the deposition front control the evolution and stability of the hydrogen bubbles. The unusual high deposition potential measured at 18 mA cm^{-2} may be indicative of the conditions that led to the generation and entrapment of more hydrogen bubbles.

In spite of the very high ductility as evidenced by the fracture surfaces, the deposits showed very limited tensile elongation, which varied among the samples from the same deposit. The tensile elongation is composed of two components, the elastic and the plastic components. Due to the thinness of the samples, strain could not be measured by the use of an extensometer. Since the elongations were measured based on the crosshead speed, the actual strains are slightly smaller than the values reported. However, the plastic component, e_f^p, is believed to be accurate. The tensile samples showed no elongation after necking, that is, fracture occurred at the maximum load. This lack of post-uniform elongation may be associated with the thinness of the samples [15] and/or it may be due to the fact that metallic nanostructures have very low strain rate sensitivity and hence show limited elongation after necking [16]. The extent of uniform elongation in a tensile specimen depends on the yield strength and the strain-hardening rate. A decrease in the yield strength or an increase in the strain-hardening rate will result in improvement of the maximum uniform strain [17]. Although the samples deposited at 50 mA cm^{-2} exhibited very low yield strengths their maximum uniform strain was unusually low. For example conventional hot-rolled nickel has a yield strength of 135 to 500 MPa with a total elongation of 30 to 40% [18]. The very low uniform elongation of these deposit and the variations observed in the elongation of all samples may be attributed to the presence of atomic hydrogen in the deposits. Hydrogen is known to segregate to dislocation cores and reduce the friction stress as well as promoting localized deformation [19], which causes premature plastic instability and necking.

3.4. *Effect of current density*

The results of this study confirmed that increasing the current density increases the grain size of nickel deposits. Assuming that the overpotential increases with the applied current density, one would expect the nucleation rate to increase with increased current density. However, the overpotential measured (Table 1) decreased with increasing current density from 18 to 25 mA cm^{-2} and then increased when the current density was raised to 50 mA cm^{-2}. This behaviour suggests a complex cur-

rent–electrode potential relationship and a lack of correlation between the grain size and the measured potential.

Cziráki et al. [8] attributed the increase in the grain size of the nickel deposited from a nickel sulfate solution and at relatively high current densities to a decrease in the concentration of Ni ions at the deposit–electrolyte interface. Our results show that the efficiency of nickel deposition decreased with increasing current density, which can be interpreted as a relative decrease in the Ni ion concentration. Nevertheless, the total deposition rate (product of current density and efficiency) still increased with the applied current density. Assuming that the codeposition of hydrogen is the dominant side reaction, the decrease in efficiency with increasing the current density is indicative of a higher rate of hydrogen formation at the cathode surface. Haug and Jenkins [20] have shown that hydrogen decreases the surface energy of the {100} crystallographic planes preferentially and encourages planar growth in nickel. Therefore, it is plausible that the modification of the growth interface by hydrogen facilitates the formation of larger grains. This mechanism is also consistent with the unusually low yield strength and maximum uniform elongation observed in the 50 mA cm^{-2} sample as discussed in the previous section.

4. Summary and conclusions

The objective of this study was to investigate the effect of current density on the microstructure and mechanical properties of electrodeposited nanocrystalline nickel. The deposition was conducted galvanostatically at 18, 25 and 50 mA cm^{-2} in a nickel sulfamate solution using a conventional rotating disc set up with annealed copper as the substrate. Analysis of the results led to the following conclusions:

(i) Increasing the current density results in an increase in the average crystallite size of the nickel deposits. This phenomenon is associated with a drop in the deposition efficiency and the evolution of more hydrogen at the cathode interface. The changes in the surface energy and growth mechanisms in the presence of hydrogen are suggested as being responsible for the increase in the crystallite size.

(ii) The nickel deposits showed a (100) texture on the substrate side whose strength deceased through the thickness of the deposits. An excellent correlation between the decrease in the crystallite size and the loss of texture was found.

(iii) The strength and strain-hardening rate values increased with grain refinement.

(iv) The nickel deposits were very ductile as evaluated by their fracture behaviour. Nevertheless, their tensile elongations were low and not consistent between the samples tested from the same deposit. The low elongation of the deposit made at 18 mA cm^{-2} is believed to be due to the entrapment of hydrogen bubbles. The unexpectedly low tensile elongation of the sample deposited at 50 mA cm^{-2} is suggested to be due to the incorporation of atomic hydrogen in the deposit.

Acknowledgement

This research was supported by the National Science Foundation under the grant DMR-9980213.

References

1. F. Ebrahimi, D. Kong, T.E. Matthews and Q. Zhai, *in* T.S. Srivastan and K.A. Khor (Eds), Processing and Fabrication of Advanced Materials VII, (TMS Publication, Warrendale, PA, 1998), p. 509.
2. H.D. Merchant, *in* H.D. Merchant (Ed.), 'Defect Structure, Morphology and Properties of Deposits', (TMS Publication, Warrendale, PA, 1995), p. 1.
3. A.R. Despić, *in* J.O.M. Bockris, B.E. Conway and E. Yeager (eds.) 'Comprehensive Treatise of Electrochemistry', Vol. 7 (Plenum, New York, 1983), Chapter 76.
4. L. Oniciu and L. Mureşan, *J. Appl. Electrochem.* **21** (1991) 565.
5. J.K. Dennis and J.J. Fuggle, *Electroplat. Metal Finish.* Jan. (1968) 17.
6. F. Ebrahimi, G.R. Bourne, M.S. Kelly and T.E. Matthews, *NanoStructured Mater.* **11**(3) (1999) 343.
7. W. Schmickler, 'Interfacial Electrochemistry' (OUP, Oxford, 1996), p. 129.
8. Á. Cziráki, B.F. Fogarassy, I. Geröcs, E. Töth-Kádár and I. Bakonyi, *J. Mater. Sci.* **29** (1994) 4771.
9. F. Ebrahimi and Q. Zhai, *Mater. Sci. Eng. A* **255** (1998) 20.
10. D.M. Tench and J.T. White, *J. Electrochem Soc.* **137** (1990) 3061.
11. F. Ebrahimi and A.J. Liscano, *Mater. Sci. Eng. A* **301** (2001) 23.
12. F. Ebrahimi and Z. Ahmed, 'The effect of substrate on the microstructure and tensile properties of electrodeposited nanocrystalline nickel,' Materials characterization Journal, in press (2003).
13. J.R. Weertman and P.G. Sanders, *Solid State Phenomena* **35–36** (1994) 249.
14. S. Nakahara and Y. Okinaka, *Acta Metall.* **31** (1993) 713.
15. M. Klein, A. Hardrboletz, B. Weiss and G. Khatibi, *Mater. Sci Eng. A* **319–321** (2001) 924.
16. F. Ebrahimi, Q. Zhai and D. Kong, *Scripta Materialia* **39** (1998) 315.
17. D.K. Matlock, F. Zia-Ebrahimi and G. Krauss, *in* 'Deformation, Processing and Structure', 1982 Materials Science Seminar (ASM Publication, 1984), pp. 47–83.
18. 'ASM Handbook', Vol. 2, 10th ed (1990).
19. H.K. Birnbaum and P. Sforonis, *Mater. Sci. Eng. A* **176** (1994) 191.
20. K. Haug and T. Jenkins, *J. Phys. Chem. B* **104** (2000) 10017.